Gold Nanoplates

DOI: 10.1002/anie.201105850

Synthesis of Gold Square-like Plates from Ultrathin Gold Square Sheets: The Evolution of Structure Phase and Shape**

*Xiao Huang, Hai Li, Shaozhou Li, Shixin Wu, Freddy Boey, Jan Ma, and Hua Zhang**

Gold nanostructures (AuNSs) have been studied intensively because of their unique chemical and physical properties,[1] which make them promising candidates in various applications.[2] Anisotropic AuNSs, in particular, are receiving special attention, owing to their special properties related to their shape, size, and crystallinity.[3] For example, Au nanorods exhibit size-tunable surface plasma resonance (SPR) in the visible and near-infrared (NIR) regimes, resulting in their applications in biological imaging and cancer therapy.[4]

Understanding how crystals grow in solution is of great importance for the shape- and size-controlled synthesis of anisotropic nanostructures. Noble-metal nanostructures have been used as prototypes to study crystal growth and shape evolution.[5] For example, previous studies have investigated the evolution of Au nanocrystals from decahedrons to cubes[5c] or from nanorods to octahedrons.[5a] Fine-tuning of the growth kinetics at different crystal planes has shown to be critical for the shape-controlled synthesis.[6] This kinetic control can be realized by, for example, using surface capping molecules[7] and foreign ions.[8]

However, the aforementioned studies only investigated AuNSs of the single face-centered cubic (fcc) phase, or those containing a dominant fcc phase with a small amount of hexagonal close-packed (hcp) crystal defects, for example, twins and stacking faults.[6] Recently, silver nanostructures (AgNSs) with mixed hcp and fcc phases (with comparable amounts of each) have been reported.[9] The introduction of such structures with unusual phases has led to the formation of unique AgNS architectures that are different from those with the common fcc phase.[9a,c] This difference in morphology arises from the dimension variation related to the phase energies.[9b] Although the synthesis of some hcp/fcc mixed AgNSs has been successful, little is known about how these structures evolve from nucleation in the solution phase. Therefore, it is very important to understand the shape as well as the phase development in the noble-metal nanostructures.

[*] Dr. X. Huang, Dr. H. Li, Dr. S. Li, Dr. S. Wu, Prof. F. Boey, Prof. J. Ma, Prof. H. Zhang
School of Materials Science and Engineering
Nanyang Technological University
50 Nanyang Avenue, Singapore 639798 (Singapore)
E-mail: hzhang@ntu.edu.sg
hzhang166@yahoo.com
Homepage: http://www.ntu.edu.sg/home/hzhang/

[**] This work was supported by AcRF Tier 2 (ARC 10/10, No. MOE2010-T2-1-060) from MOE and New Initiative Fund FY 2010 (M58120031) from NTU in Singapore.

Supporting information for this article is available on the WWW under http://dx.doi.org/10.1002/anie.201105850.

Recently, graphene has attracted increasing research interest, owing to its outstanding physical properties.[10] Its derivatives, such as graphene oxide (GO) and reduced graphene oxide (rGO), can be produced in large amounts by facile procedures, thus giving many applications in a variety of fields.[10a] For example, by using GO[11] or rGO[12] as template, many noble-metal nanostructures have been synthesized. However, the obtained nanostructures were mostly spherical or randomly shaped. Recently, for the first time, we synthesized ultrathin hcp Au square sheets (AuSSs) on GO sheets.[13]

Herein, we report the synthesis of Au square-like plates (AuSPs) from the hcp AuSSs through a secondary growth step. These AuSPs contain alternating hcp and fcc structural domains, which induce the thickness variation in each AuSP. To the best of our knowledge, this is the first time that the shape and phase evolution of an AuNS from exclusively hcp phase to an alternating hcp/fcc structure has been demonstrated; the formation of this structure results from the interplay of kinetic growth and phase stability. Importantly, novel Au architectures can be fabricated when new structural phases are introduced, and these structures might possess unique chemical and physical properties for future applications.[14]

The detailed synthesis of AuSPs using a secondary growth method is described in the Experimental Section. Briefly, the ultrathin AuSSs were synthesized by our previous method with a minor modification,[13] by heating a solution of $HAuCl_4$ (4 mM) and 1-amino-9-octadecene (170 mM) in a mixed solvent of hexane and ethanol at 58 °C for 14 h. The obtained AuSSs (Figure 1 a) were washed and redispersed in a fresh growth solution, which contained $HAuCl_4$ (3 mM) and 1-amino-9-octadecene (140 mM), and heated at 58 °C for another 10 h. In our synthesis process, the role of 1-amino-9-octadecene molecules is shown below. First, they can be adsorbed onto the surface of GO sheets to assist the dispersion of GO in hexane, because GO sheets with oxygen-containing groups anchored on their surfaces cannot be dispersed in nonpolar solvents such as hexane.[10a,13] Second, they serve as the reducing agent by forming 1-amino-9-octadecene–AuCl complex with subsequent slow reduction of Au^+ to Au^0.[15] Third, they are the stabilizing agents that bind on the surface of formed Au nanostructures.[15]

The secondary growth process led to the formation of AuSPs with side lengths of 200–400 nm (Figure 1 b,c). The thickness of AuSP is not uniform over its basal plane, and the plate is thinner in the center and thicker at one pair of opposite edges (Figure 1 b,c and Figure 2 a). This variation of thickness is also confirmed by atomic force microscopy

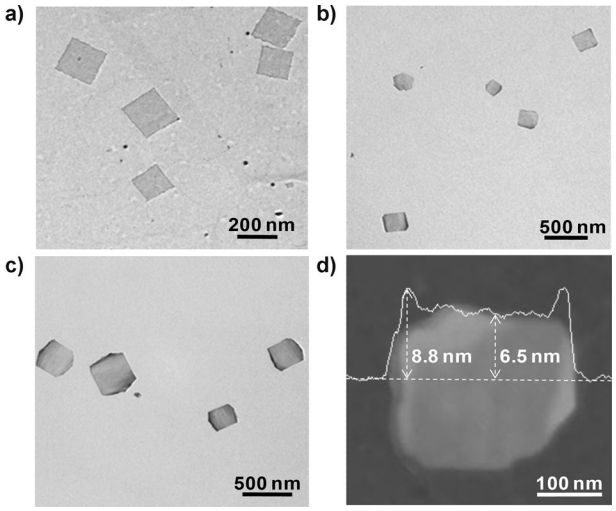

Figure 1. a) TEM image of the AuSSs synthesized on GO. b,c) TEM images of AuSPs on GO synthesized from the secondary growth of AuSSs. d) AFM image and section analysis of a typical AuSP.

(AFM) measurements (Figure 1d). The measured thicknesses of the center and edge are approximately 6.5 and 8.8 nm, respectively, which includes the thickness of surfactants (1-amino-9-octadecene) adsorbed on both sides of the AuSP. Furthermore, we estimated the thickness of the center part of an AuSP by measuring its folded edge under TEM, without the adsorbed alkyl amine molecules (Figure S1 in Supporting Information). Note that a similar method has been employed to characterize other 2D nanomaterials, such as to identify the layer number of graphene[16] and boron nitride nanosheets[17] and to determine the thickness of WS_2 and MoS_2 nanosheets.[18] Based on the estimation from the folded edge[13] of one AuSP, the thickness in the center is 5.0 ± 0.6 nm, which is approximately 1.5 nm thinner than 6.5 nm obtained by AFM (Figure 1d). We believe that this value of 1.5 nm arises from the amine molecules adsorbed on both sides of the AuSP. Therefore, after reduction of 1.5 nm, the edge of an AuSP is approximately 7.3 nm thick.

Experimental and theoretical studies have shown that when the dimension of a nanostructure decreases to a critical value, the surface energy becomes dominant in the system energy, and thus its crystal phase can deviate from that of its bulk counterpart. For example, an Au nanobridge with diameter of approximately 2 nm generated by electron beam thinning displayed an fcc core and hcp shell;[19] electrochemically deposited Ag nanowires with a diameter of approximately 30 nm showed hcp structures;[9b] and pure fcc Co nanoparticles (bulk Co has hexagonal structure) were obtained when their sizes were less than 20 nm.[20] Based on our previous observation,[13] the pure hcp-phase Au structures are only stable when they have at least one dimension less than a few nanometers (e.g. less than 6 nm in thickness for the AuSS). It is therefore predictable that the hcp-to-fcc phase transformation might have occurred during the growth of AuSP from AuSS.

Figure 2b shows the selected area electron diffraction (SAED) pattern of a typical AuSP (Figure 2a). It reveals the

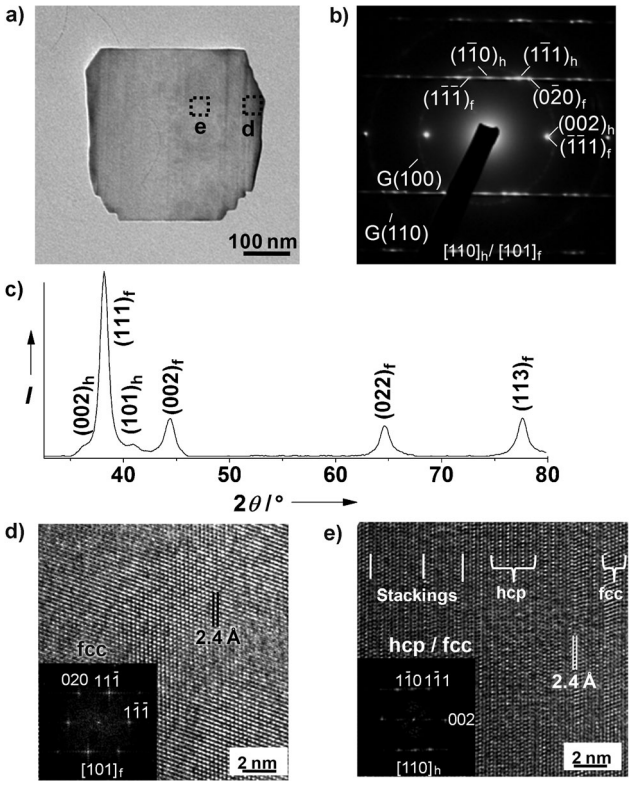

Figure 2. a) TEM image of a typical AuSP synthesized on GO. b) SAED pattern of an AuSP. c) XRD analysis of AuSPs deposited on a glass substrate, operated at the 2θ mode. d,e) HRTEM images of the areas designated in (a). Insets in (d,e): Fast Fourier transform (FFT) generated SAED patterns of the corresponding HRTEM images in (d,e).

superposition of SAED patterns of the fcc[110] and hcp[110] zone axes and streaks along the $[111]_f$ (or $[002]_h$) direction induced by the random stackings of the fcc and hcp phases. X-ray diffraction (XRD) analysis conducted at the 2θ mode (Figure 2c) shows the diffraction peaks associated with the hcp(002) (ca. 37°) and hcp(101) (ca. 41°) planes, along with those peaks for the Au fcc planes (ICPDS 4-0784), thus confirming the presence of both hcp and fcc structures. For comparison, we also conducted XRD in the $\theta/2\theta$ mode (Figure S2 in the Supporting Information), in which the substrate and detector moved by θ and 2θ, respectively. In this mode, only crystal planes parallel to the substrate were diffracted by the X-ray. This shows that the peak associated with $(022)_f$ and $(110)_h$ at approximately 65° (Figure S2 in the Supporting Information) is relatively strong compared to the standard diffraction data (ICPDS 4-0784), because it is associated with the basal plane of AuSP, which is parallel to the substrate (Figure 2b).

To further understand the crystal structures of AuSPs, high-resolution TEM (HRTEM) images (Figure 2d,e) were taken at different areas on a typical AuSP (designated in the dotted squares in Figure 2a). The edge area of the AuSP (Figure 2d) shows a defect-free fcc crystal structure viewed along the $[101]_f$ zone axis, which is confirmed by the FFT-generated SAED pattern of the corresponding area (inset in Figure 2d). On the contrary, the center area of the AuSP, which is approximately 2.3 nm thinner than the edge, shows

faulted stacking planes of both the hcp and fcc structures, further indicated by the FFT-generated SAED pattern with streaks along the $[002]_h$ direction (inset in Figure 2e). Note that hcp and fcc are both close-packed structures, and their energies are similar. Therefore, the stacking fault in one system can actually be regarded as the presence of a segment of the other. Taking the hcp phase as the reference, examples of fcc stacking faults are shown in Figure 2e, in which short-range domains of hcp and fcc structures are also marked accordingly. All these observations are in line with our previous finding that the Au hcp phase prefers to exist in thinner structures than does the fcc phase.[13]

Although AuSS and AuSP are both square-like structures, their square sides are associated with different crystal facets. The illustration in Scheme 1 shows the relative orientations of

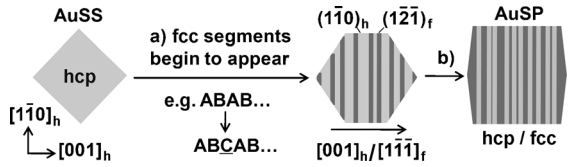

Scheme 1. Schematic illustration of the shape and phase evolution of AuSS to AuSP. hcp = light gray, fcc = dark gray.

AuSS and AuSP during the shape and phase transformation. When the AuSS is used as the seed for the secondary growth, the deposition of newly reduced Au atoms on the existing Au surface is in the $[1\bar{1}0]_h$, $[001]_h$, and $[110]_h$ directions. The growth in the $[110]_h$ direction leads to the thickness increase of the Au structure. As the Au structure grows thicker, fcc packing domains will form owing to the energy preference (step a in Scheme 1). As a result, faulted stackings begin to appear in the original hcp packing sequence, for example, from ABAB… to AB*C*AB…, which gives rise to the newly formed fcc segments. The nucleated fcc stacking faults are randomly distributed over the initial hcp structure, as shown in the HRTEM image of the center area (Figure 2e) as well as the dark-field image taken with the $[1\bar{1}0]_h$ reflection (Figure S3 in the Supporting Information). Such a lattice structure has also been observed in hcp–fcc phase transformations in ZnS[21] and CoNi alloy.[22] The formation of mixed stackings creates elastic strain in the structure at the phase interfaces,[14] which drives the faster growth in the $[001]_h$ (or $[1\bar{1}\bar{1}]_f$) direction compared to the $[1\bar{1}0]_h$ (or $[1\bar{2}\bar{1}]_f$) direction. Thus, the top and bottom edges are bound by the flat $(1\bar{1}0)_h/(1\bar{2}\bar{1})_f$ planes owing to the relatively slow growth rate normal to these planes (as viewed in the position illustrated in Scheme 1). Hexagon-like structure can be observed at some intermediate stage when the reaction has occurred for approximately 7 h (Figure S4 in the Supporting Information). This hexagon-like structure, when its top and bottom edges grew wider along the $[001]_h/[1\bar{1}\bar{1}]_f$ direction, eventually develops into the square-like structure, that is, the AuSP (step b in Scheme 1).

Recall that one pair of the opposite edges of an AuSP, which is along the $[001]_h$ direction, is thicker than the center part of the structure. The possible explanation for this phenomenon is that once the fcc packing domains have appeared at the edge parts, they continue to expand both laterally and vertically to form the defect-free fcc lattice structure. However, in the center part, which contains both the hcp and fcc domains, the continuous increase in the thickness requires additional energy for the phase transformation from hcp to fcc. Therefore, the increase of thickness at the edge is faster than in the center. This observation demonstrates the dimension-related phase variation in nanostructures, which has also been found in the rod–needle and plate–belt heterogeneous Ag structures,[9a] InAs nanowires,[14b] and ZnSe nanowires.[23]

In summary, we have synthesized Au square-like plates (AuSPs) through the secondary growth of hcp Au square sheets (AuSSs) on GO. The AuSPs contain the alternating hcp/fcc structural domains in the center and defect-free fcc domains at one pair of the opposite thick edges. For the first time, we demonstrate the phase transformation from hcp to fcc associated with shape variation in Au nanostructures (AuNSs). We believe that the noble-metal nanostructures with unusual crystal might have novel physical and chemical properties. Furthermore, in the future, AuNSs with novel morphologies can be designed and synthesized based on the hcp/fcc polymorphs.

Experimental Section

Chemicals: Natural graphite (SP-1) was purchased from Bay Carbon (Bay City, MI, USA) and used for synthesis of graphene oxide (GO). Potassium permanganate (Sigma–Aldrich, Milwaukee, WI, USA), H_2SO_4 (98%, Sigma–Aldrich, Milwaukee, WI, USA), ethanol (99.9%, absolute, Merck), hexane (technical grade, Sigma–Aldrich, Milwaukee, WI, USA), 1-amino-9-octadecene ($CH_3(CH_2)_7CH{=}CH(CH_2)_8NH_2$, 70%, technical grade, Sigma–Aldrich, Milwaukee, WI, USA), and hydrogen tetrachloroaurate(III) (ACS, 99.99%, Alfa Aesar) were used without further purification.

Synthesis of graphene oxide (GO): All glassware was washed with agua regia ($HCl/HNO_3 = 3{:}1$ v:v) and rinsed with Milli-Q water, ethanol, and then Milli-Q water again (**CAUTION**: Aqua regia is a very corrosive oxidizing agent, which should be handled with extreme care). Graphite oxide was synthesized from natural graphite (SP-1) by the modified Hummers method.[11] The obtained graphite oxide was dispersed in water or ethanol with a defined concentration and subsequently sonicated to give GO.

Synthesis of Au square sheets (AuSSs) on GO: The AuSSs were synthesized based on our recently reported method with a minor modification.[13] Briefly, GO in ethanol (0.5 mL, 0.2 mg mL^{-1}) was centrifuged and re-dispersed in the growth solution (2 mL) containing $HAuCl_4$ (4 mM) and 1-amino-9-octadecene (170 mM) in a mixture of hexane and ethanol (23:2 v:v). The growth was heated in a water bath at 58°C for 14 h to obtain the AuSSs on GO. The resulting solution was centrifuged at 5000 rpm for 10 min and washed three times with hexane.

Synthesis of Au square-like plates (AuSPs) on GO: The above AuSS solution in hexane was centrifuged and re-dispersed in a fresh growth solution (2 mL) containing $HAuCl_4$ (3 mM) and 1-amino-9-octadecene (140 mM) in a mixture of hexane and ethanol (23:2 v:v). The growth solution was heated in a water bath at 58°C for 10 h to obtain the AuSPs on GO. The final solution was centrifuged at 3500 rpm for 8 min and washed three times with hexane prior to further characterization.

Characterization: A drop of a solution containing the Au nanostructures on GO sheets was placed on a holey-carbon-coated

copper grid, Si/SiO_2, and glass slide, and then dried in air prior to characterization by transmission electron microscopy (TEM, JEM 2010F), atomic force microscopy (AFM, Dimension 3100 Veeco, CA), and X-ray diffraction (XRD, Shimadzu), respectively.

Received: August 18, 2011
Published online: November 3, 2011

Keywords: fcc structures · gold · hcp structures · phase transformation · template synthesis

[1] a) J. E. Millstone, S. J. Hurst, G. S. Métraux, J. I. Cutler, C. A. Mirkin, *Small* **2009**, *5*, 646 – 664; b) M. Hu, J. Chen, Z.-Y. Li, L. Au, G. V. Hartland, X. Li, M. Marquez, Y. Xia, *Chem. Soc. Rev.* **2006**, *35*, 1084 – 1094.

[2] a) N. L. Rosi, D. A. Giljohann, C. S. Thaxton, A. K. R. Lytton-Jean, M. S. Han, C. A. Mirkin, *Science* **2006**, *312*, 1027 – 1030; b) R. Narayanan, M. A. El-Sayed, *J. Phys. Chem. B* **2005**, *109*, 12663 – 12676.

[3] a) H. Yuan, W. Ma, C. Chen, J. Zhao, J. Liu, H. Zhu, X. Gao, *Chem. Mater.* **2007**, *19*, 1592 – 1600; b) C. J. Murphy, *J. Phys. Chem. B* **2005**, *109*, 13857 – 13870; c) S. Link, M. A. El-Sayed, *Int. Rev. Phys. Chem.* **2000**, *19*, 409 – 453.

[4] a) X. H. Huang, I. H. El-Sayed, W. Qian, M. A. El-Sayed, *J. Am. Chem. Soc.* **2006**, *128*, 2115 – 2120; b) L. F. Gou, C. J. Murphy, *Chem. Mater.* **2005**, *17*, 3668 – 3672.

[5] a) Y. Xiang, X. Wu, D. Liu, L. Feng, K. Zhang, W. Chu, W. Zhou, S. Xie, *J. Phys. Chem. C* **2008**, *112*, 3203 – 3208; b) F. R. Fan, D. Y. Liu, Y. F. Wu, S. Duan, Z. X. Xie, Z. Y. Jiang, Z. Q. Tian, *J. Am. Chem. Soc.* **2008**, *130*, 6949 – 6951; c) E. Dovgolevsky, H. Haick, *Small* **2008**, *4*, 2059 – 2066; d) Y. Ding, F. Fan, Z. Tian, Z. L. Wang, *Small* **2009**, *5*, 2812 – 2815.

[6] a) Y. Xia, Y. Xiong, B. Lim, S. E. Skrabalak, *Angew. Chem.* **2009**, *121*, 62 – 108; *Angew. Chem. Int. Ed.* **2009**, *48*, 60 – 103; b) A. R. Tao, S. Habas, P. Yang, *Small* **2008**, *4*, 310 – 325.

[7] a) D. Seo, J. C. Park, H. Song, *J. Am. Chem. Soc.* **2006**, *128*, 14863 – 14870; b) T. K. Sau, C. J. Murphy, *J. Am. Chem. Soc.* **2004**, *126*, 8648 – 8649.

[8] a) J. E. Millstone, W. Wei, M. R. Jones, H. Yoo, C. A. Mirkin, *Nano Lett.* **2008**, *8*, 2526 – 2529; b) M. Z. Liu, P. Guyot-Sionnest, *J. Phys. Chem. B* **2005**, *109*, 22192 – 22200.

[9] a) X. S. Shen, G. Z. Wang, X. Hong, X. Xie, W. Zhu, D. P. Li, *J. Am. Chem. Soc.* **2009**, *131*, 10812 – 10813; b) X. Liu, J. Luo, J. Zhu, *Nano Lett.* **2006**, *6*, 408 – 412; c) H. Liang, H. Yang, W. Wang, J. Li, H. Xu, *J. Am. Chem. Soc.* **2009**, *131*, 6068 – 6069.

[10] a) X. Huang, Z. Y. Yin, S. X. Wu, X. Y. Qi, Q. Y. He, Q. C. Zhang, Q. Y. Yan, F. Boey, H. Zhang, *Small* **2011**, *7*, 1876 – 1902; b) X. Huang, X. Qi, F. Boey, H. Zhang, *Chem. Soc. Rev.* **2012**, DOI: 10.1039/C1CS15078B.

[11] X. Zhou, X. Huang, X. Qi, S. Wu, C. Xue, F. Y. C. Boey, Q. Yan, P. Chen, H. Zhang, *J. Phys. Chem. C* **2009**, *113*, 10842 – 10846.

[12] X. Huang, X. Z. Zhou, S. X. Wu, Y. Y. Wei, X. Y. Qi, J. Zhang, F. Boey, H. Zhang, *Small* **2010**, *6*, 513 – 516.

[13] X. Huang, S. Li, Y. Huang, S. Wu, X. Zhou, S. Li, C. L. Gan, F. Boey, C. A. Mirkin, H. Zhang, *Nat. Commun.* **2011**, *2*, 292.

[14] a) X. S. Fang, C. H. Ye, L. D. Zhang, T. Xie, *Adv. Mater.* **2005**, *17*, 1661 – 1665; b) P. Caroff, K. A. Dick, J. Johansson, M. E. Messing, K. Deppert, L. Samuelson, *Nat. Nanotechnol.* **2009**, *4*, 50 – 55.

[15] a) Y. Ma, J. Zeng, W. Li, M. McKiernan, Z. Xie, Y. Xia, *Adv. Mater.* **2010**, *22*, 1930 – 1934; b) Z. Li, J. Tao, X. Lu, Y. Zhu, Y. Xia, *Nano Lett.* **2008**, *8*, 3052 – 3055; c) X. M. Lu, M. S. Yavuz, H. Y. Tuan, B. A. Korgel, Y. N. Xia, *J. Am. Chem. Soc.* **2008**, *130*, 8900 – 8901; d) Z. Y. Huo, C. K. Tsung, W. Y. Huang, X. F. Zhang, P. D. Yang, *Nano Lett.* **2008**, *8*, 2041 – 2044.

[16] J. C. Meyer, A. K. Geim, M. I. Katsnelson, K. S. Novoselov, T. J. Booth, S. Roth, *Nature* **2007**, *446*, 60 – 63.

[17] H. Zeng, C. Zhi, Z. Zhang, X. Wei, X. Wang, W. Guo, Y. Bando, D. Golberg, *Nano Lett.* **2010**, *10*, 5049 – 5055.

[18] H. S. S. R. Matte, A. Gomathi, A. K. Manna, D. J. Late, R. Datta, S. K. Pati, C. N. R. Rao, *Angew. Chem.* **2010**, *122*, 4153 – 4156; *Angew. Chem. Int. Ed.* **2010**, *49*, 4059 – 4062.

[19] Y. Kondo, K. Takayanagi, *Phys. Rev. Lett.* **1997**, *79*, 3455.

[20] O. Kitakami, H. Sato, Y. Shimada, F. Sato, M. Tanaka, *Phys. Rev. B* **1997**, *56*, 13849.

[21] M. Sebastian, P. Krishna, *Pramana* **1984**, *23*, 395 – 403.

[22] C. Hitzenberger, H. P. Karnthaler, A. Korner, *Acta Metall.* **1988**, *36*, 2719 – 2728.

[23] Q. Li, X. Gong, C. Wang, J. Wang, K. Ip, S. Hark, *Adv. Mater.* **2004**, *16*, 1436 – 1440.

